Exact Analytic Spectra of Asymmetric Modulation Instability in Systems with Self-Steepening Effect

Chong Liu,[1,2,3,4,*] Yu-Han Wu,[1] Shao-Chun Chen,[1] Xiankun Yao,[1] and Nail Akhmediev[2,†]
[1]School of Physics, Northwest University, Xi'an 710127, China
[2]Optical Sciences Group, Department of Theoretical Physics, Research School of Physics, The Australian National University, Canberra, Australian Capital Territory 2600, Australia
[3]Shaanxi Key Laboratory for Theoretical Physics Frontiers, Xi'an 710127, China
[4]NSFC-SPTP Peng Huanwu Center for Fundamental Theory, Xi'an 710127, China

(Received 24 September 2020; revised 16 April 2021; accepted 19 July 2021; published 27 August 2021)

Nonlinear waves become asymmetric when asymmetric physical effects are present within the system. One example is the self-steepening effect. When exactly balanced with dispersion, it leads to a fully integrable system governed by the Chen-Lee-Liu equation. The latter provides a natural basis for the analysis of asymmetric wave dynamics just as nonlinear Schrödinger or Korteweg–de Vries equations provide the basis for analyzing solitons with symmetric profile. In this work, we found periodic wave trains of the Chen-Lee-Liu equation evolved from fully developed modulation instability and analyzed a highly nontrivial spectral evolution of such waves in analytic form that shows strong asymmetry of its components. We present the conceptual basis for finding such spectra that can be used in analyzing asymmetric nonlinear waves in other systems.

DOI: 10.1103/PhysRevLett.127.094102

Asymmetric nonlinear waves are common in hydrodynamics and in optics. Examples include undular bores [1], morning glory phenomenon [2], dispersive shock waves in optics [3], optical wave breaking [4], and multiplicity of other phenomena in nature and in laboratory settings [5,6]. Ocean waves are naturally nonlinear and asymmetric with steep front and smooth tail [7]. Exact analytic description of asymmetric waves is a challenge that so far has not been fully resolved. There are evolution equations with nonlinear terms responsible for the wave asymmetry such as the Sasa-Satsuma equation (SSE) [8]. However, the SSE contains a mix of symmetric and asymmetric nonlinear terms with their relative contributions that cannot be easily singled out. One of the equations that allows us to study the asymmetry of nonlinear waves caused solely by the self-steepening effect is the Chen-Lee-Liu equation (CLLE) [9]. The self-steepening term in the CLLE is due to the intensity dependent group velocity [10,11]. In optics, it appears through the interplay of quadratic and cubic nonlinearities in frequency-doubling crystals [12]. It has been shown that the CLLE describes phase-mismatched second-harmonic waves [13] and nonlinear waves in quadratic nonlinear media [14,15]. Validity of the CLLE in optics has been demonstrated experimentally [16].

Significance of the CLLE also lies in its integrability [9]. This means that its solutions can be presented analytically. Moreover, based on the accurate balance of only two physical effects—dispersion and self-steepening, this equation can be considered as one of the fundamental evolution equations like the Korteweg–de Vries (KdV) or nonlinear Schrödinger equations (NLSEs). However, in contrast to the KdV and the NLSEs, it describes asymmetric waves thus dealing with a different class of phenomena. In this Letter, we consider periodic waves of CLLE that are asymmetric. As in other nonlinear media, periodic waves may emerge "from nowhere" due to modulation instability (MI) [17]. Because of this feature, MI is one of the key processes studied in nonlinear physics. It is at the origin of solitons inception [18], supercontinuum generation [19], and rogue wave events [20]. It is presently known as Benjamin-Fair instability [21] in the case of water waves or Bespalov-Talanov instability [22] in the case of optical beams. In each case, the nonlinear stage of the MI scenario is provided by the "Akhmediev breather" (AB) [23,24]. The latter is an exact analytical solution of the standard NLSE [25], which describes exactly both the process of the initial growth of periodic perturbation and the following full scale recurrent evolution back to the continuous wave. The AB theory provides analytical results for the evolution of multiplicity of the spectral sidebands, which is beyond the reach of the truncated approach [26]. Because of these unique properties, the NLSE AB has led to successful studies of the Fermi-Pasta-Ulam recurrence [27,28], supercontinuum generation [29,30], higher-order MI effect [31], the nonlinear phase shift [32], and created the basis for experiments on rogue waves excitation [33].

In all these findings, the AB exhibits conspicuous reflection symmetry in both the time and the frequency domains. On the other hand, there is increasing numerical

and experimental evidence that MI can reveal broken reflection symmetry at the nonlinear stage of evolution [29,30,34,35]. Such broken symmetry constitutes a highly nontrivial part of spontaneous symmetry breaking in physics [36]. It is generally attributed to coupling nonlinear terms in the equations or higher-order effects in the model [36]. The latter include the higher-order dispersion, self-steepening, and stimulated Raman scattering. Despite being vigorously investigated, they continue to pose major challenges in our understanding of the nonlinear phenomena [37,38]. The complications arise from the fact that the higher-order terms generally break the integrability of the resulting generalized NLSE extensions. This prevents or causes difficulties in finding exact solutions.

In principle, infinitely many higher-order terms can be added to the NLSE in such a way that the corresponding equation remains integrable [39–42]. Despite being cumbersome, these extensions admit exact solutions. Some extensions of the infinite hierarchy like Hirota or Sasa-Satsuma equations result in the skewed MI dynamics, although many others keep them symmetric [42].

The dimensionless CLLE can be written in the form [9]

$$i\frac{\partial\psi}{\partial z}+\frac{\partial^2\psi}{\partial t^2}+i|\psi|^2\frac{\partial\psi}{\partial t}=0, \tag{1}$$

where $\psi(z,t)$ is the complex wave envelope, z and t are the propagation and transverse (or retarded time) variables, respectively. The last term in the left hand side $(i|\psi|^2\partial\psi/\partial t)$ describes the effect of self-steepening.

Generation of periodic waves in nonlinear media governed by Eq. (1) is described by the AB solutions of the CLLE (1). In [43], using the Darboux transformation we have shown the asymmetry of superregular breathers. Here, using the same technique, we derived a family of single AB solutions with free parameters controlling the wave train. This family can also be obtained from a more general set of breathers given by Eq. (23) in [43]. In concise form, the solution can be written as

$$\psi=(\psi_a-1)\psi_0, \tag{2}$$

where $\psi_0=a\exp[i(qt-(q^2+a^2q)z)]$ denotes the continuous wave background of the CLLE with a and q being its amplitude and frequency, respectively, and

$$\psi_a=\frac{2\sin\alpha\cosh\boldsymbol{\gamma}+2i\rho(\rho\sinh\boldsymbol{\gamma}+\sin\boldsymbol{\kappa})}{\epsilon\cosh\boldsymbol{\gamma}-\epsilon\rho\cos\boldsymbol{\kappa}-i(\sinh\boldsymbol{\gamma}-\rho\sin\boldsymbol{\kappa})}, \tag{3}$$

with $\boldsymbol{\gamma}=\gamma z=(a^4\sin 2\alpha)z/2$, $\boldsymbol{\kappa}=\kappa t=(a^2\sin\alpha)t$, $\rho=\sqrt{\cos\alpha}$, $\epsilon=\cot(\alpha/2)$. Here, α is a real parameter in the region $(0,\pi/2)$, which determines the modulation frequency $\kappa=a^2\sin\alpha$ and MI growth rate $\gamma=(a^4\sin 2\alpha)/2$. According to Eq. (2), the breather has a maximum amplitude $|\psi_{\max}|=a(1+2\rho)$ and a minimum amplitude $|\psi_{\min}|=0$.

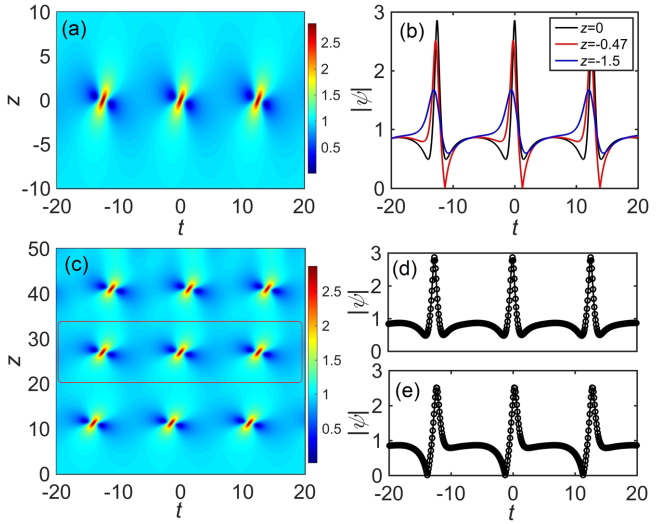

FIG. 1. (a) Amplitude distribution $|\psi(z,t)|$ of ABs given by Eq. (2). (b) Wave profiles of the solution shown in (a) at different z. The AB parameters are $a=1$, $q=-0.5$, $\alpha=\pi/6$. (c) Numerical MI dynamics starting from the weakly periodic initial condition, Eq. (5). (d) and (e) Comparison between the wave profiles of the second recurrence in (c) (framed by black solid curve) at two different z obtained numerically (circles) and the analytical solution (lines). The parameters in the initial conditions are $\Omega=0.5$, $\phi=-6\pi/5$, $\tau_s=-3.044$, $\varepsilon=0.02$. Parameters of the AB are the same as in (a).

Figure 1(a) shows the spatiotemporal amplitude profile of the AB solution (2) in the (z,t) plane. A distinctive feature of the plot is that such AB describes the MI dynamics with broken reflection symmetry relative to the line $z=0$. Instead, from Eq. (2), it follows that the solution has the inversion symmetry, $|\psi(-z,-t)|=|\psi(z,t)|$. This symmetry is clearly visible in Fig. 1(a).

The MI stage of evolution described by the AB (2) begins from a constant background at $z\to-\infty$. It has an infinitesimally small modulation with frequency κ along the t axis. Taking into account the lowest-order periodic terms, the AB solution (2) at $z\to-\infty$ can be approximated by

$$\psi=\psi_0[1-2\sqrt{2}i\varepsilon e^{-i\alpha}\rho\sin\alpha\cos(\kappa t+\pi/4)e^{\gamma}]e^{i\theta_1}, \tag{4}$$

where ε is a small real parameter ($\varepsilon\ll 1$) and $\theta_1=\alpha-\pi$ is the initial phase of the plane wave as $z\to-\infty$. This plane wave has a periodic modulation with a phase shift equal to $-\pi/(4\kappa)$. The exponential factor e^{γ} shows that this initial modulation grows with the growth rate γ.

The initial modulation is a symmetric function relative to the point $t=\pi/(4\kappa)$. When z increases, the modulation in (4) grows exponentially and loses this symmetry. It evolves and transforms spontaneously into a wave train with

asymmetric pulses shown in Fig. 1(b) (blue curve). This asymmetry is due to the self-steepening. For each pulse, its peak shifts toward positive t thus, increasing the steepness of the front edge of the pulse (red curve).

Physically, the group velocity of the pulse is intensity dependent (i.e., $v_g \equiv 1/|\psi|^2$) such that the peak of the pulse moves at a lower speed than its wings. In other words, the degree of asymmetry increases with propagation. The asymmetry is maximal when the minimal amplitude of the wave profile reaches zero [red solid line in Fig. 1(b)]. This profile can be considered as a "periodic shock wave sequence" emerging from a weakly modulated plane wave due to the MI. However, from this point, the degree of asymmetry sharply decreases while the wave amplitude continues to grow. The amplitude reaches its maximum at $z = 0$. The wave train shown by the black solid line in Fig. 1(b) becomes symmetric. The process is reversed at positive values of z. The system returns to its initial state of a weakly modulated plane wave at $z \to \infty$ with the opposite values of the time shift $\pi/(4\kappa)$ and the phase $\theta_2 = \pi - \alpha$ at $z \to \infty$.

The total phase shift $\Delta\theta$ between the initial ($z \to -\infty$) and final ($z \to \infty$) states of evolution can be calculated exactly from Eq. (2): $\Delta\theta = \theta_2 - \theta_1 = 2\pi - 2\alpha$. This is a carrier phase shift caused by the wave envelope being involved in a nonlinear process, which is known as "nonlinear phase shift" (in contrast to Berry phase). This phase shift depends on the frequency of modulation. It varies from 0 to 2π within the instability band.

It is important to support the analytical results by direct numerical simulations of Eq. (1). We used as initial conditions the weakly modulated plane wave although in a simpler form than in Eq. (4). Namely, we used

$$\psi = \psi_0\{1 + \varepsilon e^{i\phi}\cos[\Omega(t - \tau_s)]\}, \tag{5}$$

where ε is a small real parameter ($\varepsilon \ll 1$) representing the weak modulation amplitude, ϕ is the phase, Ω and τ_s are the modulation frequency and time shift, respectively. The major parameters in Eq. (5) defining the AB dynamics in numerical simulations are the modulation frequency Ω and the phase ϕ. Thus, we take $\Omega = \kappa$, $\phi = \theta_1$ as in Eq. (4).

Numerical simulations of Eq. (1) were done using the split-step technique with Fourier transform for solving the linear part and the fourth-order Runge-Kutta method for solving the nonlinear part of the CLLE. In order to reduce the numerical error accumulating in the form of high-frequency noise, we multiplied the solution in the frequency domain (2) by a super-Gaussian function.

The results of numerical simulations with the initial condition (5) are shown in Fig. 1(c). Unavoidable deviation from the exact separatrix results in periodic trajectories. Three full cycles of a periodic orbit close to the separatrix can be observed in this plot. The second one is framed by a rectangular curve. The amplitude profiles in each cycle show an excellent agreement with profiles obtained from the exact AB solution. For comparison, we choose the two points in z. In one of them, the wave profile is symmetric (around $z \approx 28$). The second profile is chosen at the point where the profile has zero (around $z \approx 28.5$). These two profiles are shown in Figs. 1(d) and 1(e). The results of numerical simulations are shown by circles while the analytic results are given by solid curves.

Next, let us consider the physical spectra of the AB solutions. The t-periodic solution can be written in the form of the infinite series $\psi(z,t) = \sum_{n=0}^{\infty} A_n(z)e^{inQt}$, where the z-dependent amplitudes of spectral harmonics ($n = 0, \pm 1, \pm 2, \ldots$) are given by

$$A_n(z) = \frac{Q}{2\pi}\int_0^{2\pi/Q} \psi(z,t)e^{-inQt}dt.$$

For symmetric solutions, the technique for calculation of the spectral amplitudes is well developed [23,42,44]. However, finding the spectral amplitudes of asymmetric signals remains a challenge. Here, we provide the technique for solving this problem. First, let us define the integral

$$\mathcal{I} = \frac{Q}{2\pi}\int_0^{2\pi/Q} \psi_a(z,t)e^{-inQt}dt$$

for an asymmetric signal ψ_a. Changing variable t in the integrand to the complex one $\mathcal{Z} = e^{iQt}$ yields

$$\mathcal{I} = \frac{i}{\pi}\int_C \mathcal{J}\mathcal{Z}^{-n}d\mathcal{Z}, \tag{6}$$

where C is a contour of integration in the form of a unit circle around zero while

$$\mathcal{J} = \frac{2\sin\alpha\cosh\boldsymbol{\gamma} + 2i\rho^2\sinh\boldsymbol{\gamma} + \rho(\mathcal{Z} - \mathcal{Z}^{-1})}{\rho(\epsilon - 1)(\mathcal{Z} - \mathcal{Z}_1)(\mathcal{Z} - \mathcal{Z}_2)}, \tag{7}$$

with $\mathcal{Z}_{1,2}$ being the roots of the binomial in the denominator

$$\mathcal{Z}_j = \frac{1}{\rho(\epsilon - 1)}(\epsilon\cosh\boldsymbol{\gamma} - i\sinh\boldsymbol{\gamma} \mp \Delta), \quad j = 1, 2, \tag{8}$$

where $\Delta = \sqrt{\rho^2(1 - \epsilon^2) + (\epsilon\cosh\boldsymbol{\gamma} - i\sinh\boldsymbol{\gamma})^2}$. It is easy to see that one of the roots in (8), say $\mathcal{Z}_1$, is inside the unit circle while the other one, say $\mathcal{Z}_2$, is outside.

Before using the residue theorem for calculation of the integral, let us consider the term $\rho(\mathcal{Z} - \mathcal{Z}^{-1})$ in the numerator of $\mathcal{J}$ in Eq. (7). Clearly, the point $\mathcal{Z} = 0$ is inside the unit circle. This fact makes the calculation of the integral more difficult. It ultimately results in the asymmetry of the spectral harmonics at positive and negative frequencies. We have to consider the residue at $\mathcal{Z} = 0$, which we denote as $\mathcal{R}_0$, on a case-by-case basis: (1) When $n = 0$, we have

$$\mathcal{R}_0 = \mathcal{J}\mathcal{Z}|_{\mathcal{Z}=0} = -\frac{1}{(\epsilon-1)\mathcal{Z}_1\mathcal{Z}_2} = -\frac{1}{1+\epsilon}. \quad (9)$$

(2) When $n \leq -1$, the point $\mathcal{Z}=0$ is not a singularity in the expression $\mathcal{J}\mathcal{Z}^{-n}$, which means that $\mathcal{R}_0 = 0$. (3) When $n \geq 1$, the point $\mathcal{Z}=0$ in the expression for $\mathcal{J}\mathcal{Z}^{-n}$ is a $(n+1)$-order singularity. The residue $\mathcal{R}_0$ in this case can be calculated using the formula [45]

$$\mathcal{R}_0 = \frac{1}{n!}\frac{d^n}{d\mathcal{Z}^n}\mathcal{J}\mathcal{Z}^{-n}\mathcal{Z}^{n+1}|_{\mathcal{Z}=0} = \frac{1}{n!}\frac{d^n}{d\mathcal{Z}^n}\mathcal{J}\mathcal{Z}|_{\mathcal{Z}=0}. \quad (10)$$

On the other hand, the residue at $\mathcal{Z}=\mathcal{Z}_1$ in the expression $\mathcal{J}\mathcal{Z}^{-n}$, which we denote as $\mathcal{R}_{\mathcal{Z}_1}$, is given by $\mathcal{R}_{\mathcal{Z}_1} = \mathcal{L}\mathcal{Z}_1^{-n}$, where $\mathcal{L} = \mathcal{J}(\mathcal{Z}-\mathcal{Z}_1)|_{\mathcal{Z}=\mathcal{Z}_1}$. The explicit expression for $\mathcal{L}$ is

$$\mathcal{L} = \frac{1}{2\Delta}[2\sin\alpha\cosh\boldsymbol{\gamma} + 2i\rho^2\sinh\boldsymbol{\gamma} + \rho(\mathcal{Z}_1 - \mathcal{Z}_1^{-1})]. \quad (11)$$

Collecting the results above and applying the residue theorem to the integral (6), we have $\mathcal{I} = -2(\mathcal{R}_0 + \mathcal{R}_{\mathcal{Z}_1})$. Thus, for the central component ($n=0$), we have

$$A_0(z) = -2\mathcal{L} - \frac{1-\epsilon}{1+\epsilon}, \quad (12)$$

while for the sidebands (the harmonics), we have

$$A_n(z) = -2\mathcal{L}\mathcal{Z}_1^{-n} + \mathcal{F}, \quad (13)$$

where $\mathcal{F} = \begin{cases} 0, & n \leq -1, \\ -2(1/n!)(d^n/d\mathcal{Z}^n)\mathcal{J}\mathcal{Z}|_{\mathcal{Z}=0}, & n \geq 1. \end{cases}$

Equations (12) and (13) describe explicitly the evolution of the infinite number of spectral components. In particular, Eq. (13) clearly shows that the spectral amplitudes of harmonics are asymmetric with respect to the central component.

Figure 2 shows the evolution of the AB spectral amplitudes according to (a) our analytical solutions and (b) numerical simulations. Remarkably, in each case, this is an *asymmetric* discrete spectrum. The energy of the central mode spreads asymmetrically to the sidebands during the MI growth-decay cycle. At the initial stage of the MI with the exponential growth of modulation, the energy is transferred from the central mode to the two nearest sidebands. However, due to the self-steepening effect, the sideband amplitudes at positive and negative frequencies are asymmetric relative to the pump. The asymmetry increases closer to the point of maximum modulation. At the very point of the maximum modulation, the energy of the central mode reaches its minimum while the energy of each higher-order harmonic reaches its maximum. The process is reversed beyond this point and the system returns to its initial state of a plane wave at $z \to \infty$. Just as in the time domain, the analytical AB spectrum exhibits one growth-return cycle. In the case of numerical simulations, the spectrum is periodic. It contains three full periods of evolution.

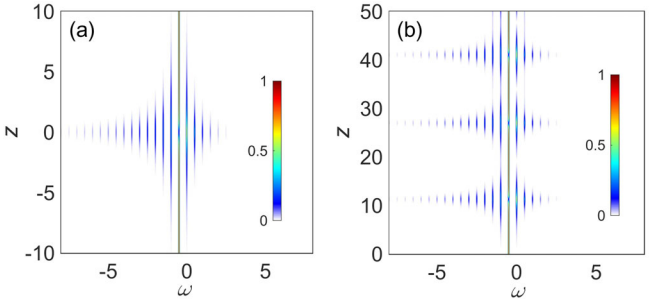

FIG. 2. (a) Analytical AB spectrum given by Eqs. (12) and (13). This corresponds to the AB evolution in z shown in Fig. 1(a). (b) Numerical AB spectrum that corresponds to the AB evolution in z shown in Fig. 1(c). The spectra are asymmetric relative to the central component.

To further understand the asymmetry of the AB spectra, we explore them in the phase plane $(|A_{\pm n}|\cos\phi_{\pm n}, |A_{\pm n}|\sin\phi_{\pm n})$, where $A_{\pm n}$ denotes the spectral amplitude and $\phi_{\pm n}$ is the corresponding phase. In Fig. 3, we compare the results of the numerical simulations and the spectral components calculated analytically, up to the third harmonic $n = \pm 3$. The second period is chosen for comparison, although, for each period of the numerical simulations the data show excellent agreement with the analytical AB spectra.

The phase trajectory of the central spectral mode in Fig. 3(a) is an unclosed curve. The starting and ending points of the curve are different. This is due to the nonlinear phase shift defined by $\Delta\theta$. On the other hand, the phase

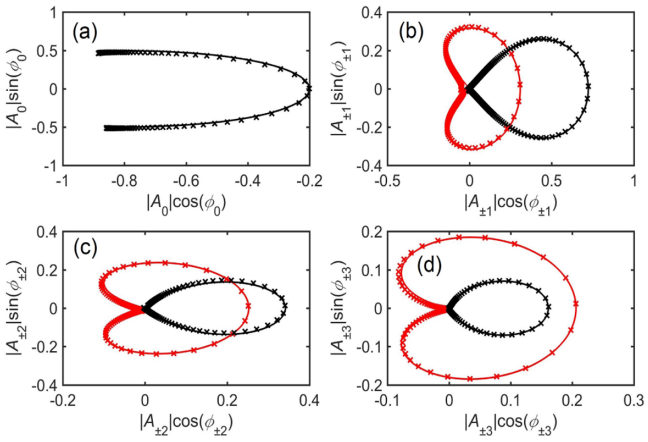

FIG. 3. The evolution of the AB spectral components on the $(|A_{\pm n}|\cos\phi_{\pm n}, |A_{\pm n}|\sin\phi_{\pm n})$ plane, up to $n = \pm 3$. Analytical results are depicted in solid lines. Numerical simulations are presented by crosses chosen at discrete points of the second period in Fig. 2(b). Panel (a) shows the evolution of the central frequency component. Panels (b)–(d) show the evolution of the nth component. Right hand side sidebands ($n > 0$) are shown in black while the left hand side sidebands ($n < 0$) are shown in red.

trajectories of the sidebands shown in Figs. 3(b)–3(d) start and end at the same point (at the origin). Their shape depends on the order of the spectral component $\pm n$. Moreover, in contrast to the symmetric spectra of the NLSE ABs, when the sideband pairs share the same orbit, the phase trajectories of sideband pairs here are asymmetric and represent different orbits. For clarity, they are shown in red and black colors in Figs. 3(b)–3(d). Positive sidebands ($n > 0$) are located on the right hand half-plane of the phase plane while negative sidebands ($n < 0$) are located in both half-planes. The size of the orbits of the sidebands decreases with increasing $|n|$.

In conclusion, we have studied analytically the dynamics of periodic wave trains governed by the CLLE that is based on the sole balance of dispersion and the self-steepening effect. As such, this equation describes the asymmetric nonlinear waves. Moreover, this equation is integrable providing the ways to find its solutions in analytic form. Thus, in mathematical physics, it has a significance of the KdV and NLSE but in contrast to them it inherently describes asymmetric waves. It was also shown that waves governed by this equation can be studied experimentally [16].

For experimental observations in optics, it is highly important to know the physical spectra of the solutions. Although integrability of the equation allowed us to find the exact AB solutions in time, it does not guarantee that the physical spectra can be also found analytically. We keep in mind that these are different from the spectra of the inverse scattering technique. Finding physical spectra of periodic solutions is a nontrivial task. This was recently demonstrated with periodic solutions of the NLSE [44]. Here, as an example, we studied the periodic waves and the AB dynamics of the CLLE and importantly, we found their spectra also analytically. Moreover, we provided here the conceptual basis for such nontrivial calculations. As far as we know, the asymmetric ABs and their physical spectra have not been presented analytically in any of the previous works.

We stress that analytic results have a clear advantage over numerical calculations. They allow one to analyze the phenomenon for the whole family of multiparameter asymmetric nonlinear waves using the analytic results in hands. Taking into account that the CLLE can be realized in experiments, the possibility of such analysis opens new ways in the studies of asymmetric nonlinear waves. The technique can also be generalized to many other models that admit the asymmetric nonlinear waves. For example, the theory can be extended to optical models with vector fields where the ABs exhibit significantly richer structures [46,47].

The work was conceived when C. L. visited Optical Sciences Group, ANU, during 2018–2019. This work is supported by National Natural Science Foundation of China (NSFC) (No. 12175178, No. 12047502, No. 12004309, and No. 11705145), and the Major Basic Research Program of Natural Science of Shaanxi Province (No. 2017KCT-12 and No. 2017ZDJC-32).

*chongliu@nwu.edu.cn
†Nail.Akhmediev@anu.edu.au

[1] N. F. Smyth and P. E. Holloway, J. Phys. Oceanogr. **18**, 947 (1988).
[2] D. R. Christie, Australian Meteorological Magazine **41**, 21 (1992).
[3] M. Conforti, F. Baronio, and S. Trillo, Opt. Lett. **37**, 1082 (2012).
[4] J. E. Rothenberg and D. Grischkowsky, Phys. Rev. Lett. **62**, 531 (1989).
[5] S. K. Ivanov, Phys. Rev. A **101**, 053827 (2020).
[6] S. Trillo, M. Klein, G. F. Clauss, and M. Onorato, Physica (Amsterdam) **333D**, 276 (2016).
[7] A. Toffoli and E. M. Bitner-Gregersen, in *Encyclopedia of Maritime and Offshore Engineering* (John Wiley & Sons, New York, 2017).
[8] N. Sasa and J. Satsuma, J. Phys. Soc. Jpn. **60**, 409 (1991).
[9] H. H. Chen, Y. C. Lee, and C. S. Liu, Phys. Scr. **20**, 490 (1979).
[10] F. DeMartini, C. H. Townes, T. K. Gustafson, and P. L. Kelley, Phys. Rev. **164**, 312 (1967).
[11] D. Anderson and M. Lisak, Phys. Rev. A **27**, 1393 (1983).
[12] J. Moses and F. W. Wise, Phys. Rev. Lett. **97**, 073903 (2006).
[13] F. Baronio, S. Chen, and D. Mihalache, Opt. Lett. **42**, 3514 (2017).
[14] S. Chen, F. Baronio, J. M. Soto-Crespo, Ph. Grelu, and D. Mihalache, J. Phys. A **50**, 463001 (2017); Y. Zhang, L. Guo, J. He, and Z. Zhou, Lett. Math. Phys. **105**, 853 (2015).
[15] H. Triki, Y. Hamaizi, Q. Zhou, A. Biswas, M. Z. Ullah, S. P. Moshokoa, and M. Belic, Optik (Stuttgart) **157**, 156 (2018).
[16] J. Moses, B. A. Malomed, and F. W. Wise, Phys. Rev. A **76**, 021802(R) (2007).
[17] J. M. Dudley, F. Dias, M. Erkintalo, and G. Genty, Nat. Photonics **8**, 755 (2014).
[18] Ch. Mahnke and F. Mitschke, Phys. Rev. A **85**, 033808 (2012).
[19] J. M. Dudley, G. Genty, and S. Coen, Rev. Mod. Phys. **78**, 1135 (2006).
[20] N. Akhmediev, A. Ankiewicz, and M. Taki, Phys. Lett. A **373**, 675 (2009).
[21] T. B. Benjamin and J. E. Feir, J. Fluid Mech. **27**, 417 (1967).
[22] V. I. Bespalov and V. I. Talanov, JETP Lett. **3**, 307 (1966).
[23] N. Akhmediev and V. I. Korneev, Theor. Math. Phys. **69**, 1089 (1986).
[24] N. Akhmediev, V. M. Eleonskii, and N. E. Kulagin, Theor. Math. Phys. **72**, 809 (1987).
[25] N. Akhmediev and A. Ankiewicz, *Solitons: Nolinear Pulses and Beams* (Chapman and Hall, London, 1997).
[26] S. Trillo and S. Wabnitz, Opt. Lett. **16**, 986 (1991).
[27] N. Akhmediev, Nature (London) **413**, 267 (2001).
[28] D. Pierangeli, M. Flammini, L. Zhang, G. Marcucci, A. J. Agranat, P. G. Grinevich, P. M. Santini, C. Conti, and E. DelRe, Phys. Rev. X **8**, 041017 (2018).
[29] J. M. Dudley, G. Genty, F. Dias, B. Kibler, and N. Akhmediev, Opt. Express **17**, 21497 (2009).

[30] N. Akhmediev, A. Ankiewicz, J. M. Soto-Crespo, and J. M. Dudley, Phys. Lett. A **375**, 775 (2011).
[31] M. Erkintalo, K. Hammani, B. Kibler, C. Finot, N. Akhmediev, J. M. Dudley, and G. Genty, Phys. Rev. Lett. **107**, 253901 (2011).
[32] N. Devine, A. Ankiewicz, G. Genty, J. M. Dudley, and N. Akhmediev, Phys. Lett. A **375**, 4158 (2011).
[33] B. Kibler, J. Fatome, C. Finot, G. Millot, F. Dias, G.Genty, N. Akhmediev, and J. M. Dudley, Nat. Phys. **6**, 790 (2010).
[34] M. Droques, B. Barviau, A. Kudlinski, M. Taki, A. Boucon, T. Sylvestre, and A. Mussot, Opt. Lett. **36**, 1359 (2011).
[35] J. M. Soto-Crespo, A. Ankiewicz, N. Devine, and N. Akhmediev, J. Opt. Soc. Am. B **29**, 1930 (2012).
[36] *Spontaneous Symmetry Breaking, Self-Trapping, and Josephson Oscillations*, edited by B. A. Malomed (Springer, Berlin-Heidelberg, 2013).
[37] D. R. Solli, G. Herink, B. Jalali, and C. Ropers, Nat. Photonics **6**, 463 (2012).
[38] S. Chen, C. Pan, Ph. Grelu, F. Baronio, and N. Akhmediev, Phys. Rev. Lett. **124**, 113901 (2020).
[39] A. Ankiewicz, D. J. Kedziora, A. Chowdury, U. Bandelow, and N. Akhmediev, Phys. Rev. E **93**, 012206 (2016).
[40] D. J. Kedziora, A. Ankiewicz, A. Chowdury, and N. Akhmediev, Chaos **25**, 103114 (2015).
[41] C. Liu, Z. Y. Yang, and W. L. Yang, Chaos **28**, 083110 (2018).
[42] A. Chowdury, A. Ankiewicz, N. Akhmediev, and W. Chang, Chaos **28**, 123116 (2018).
[43] C. Liu and N. Akhmediev, Phys. Rev. E **100**, 062201 (2019).
[44] M. Conforti, A. Mussot, A. Kudlinski, S. Trillo, and N. Akhmediev, Phys. Rev. A **101**, 023843 (2020).
[45] H. J. Weber and G. B. Arfken, *Essential Mathematical Methods for Physicists*, 5th ed. (Academic Press, New York, 2003).
[46] C. Liu, Z. Y. Yang, L. C. Zhao, and W. L Yang, Phys. Rev. A **89**, 055803 (2014).
[47] L. M. Ling and L. C. Zhao, Commun. Nonlinear Sci. Numer. Simul. **72**, 449 (2019).